Supplemental material

Arish et al., https://doi.org/10.1085/jgp.201812143

Spatial ICS analysis

Spatial ICS was used to quantify CFTR cluster density (CD) and aggregation as described in detail elsewhere (Wiseman and Petersen, 1999). Briefly, CD (i.e., the average number of independent fluorescent entities per unit area) was calculated as

$$CD = \frac{n_p}{\omega_0^2 \pi}, \quad (1)$$

where n_p is the average number of particles per image focal spot and ω_0 is the e^{-2} beam (i.e., focal spot) radius in the lateral direction. n_p is the reciprocal of the zero spatial lags amplitude of the spatial correlation function of the image, which is obtained from nonlinear least squares fitting of a 2-D Gaussian function.

The DA was calculated as

$$DA = \frac{i}{CD}, \quad (2)$$

where i is the spatial average pixel intensity for the imaged region of interest.

kICS analysis

A modification of kICS analysis was used to study CFTR membrane dynamics (Kolin et al., 2006; Pandzic, 2013; Abu-Arish et al., 2015). Briefly, the k-space temporal correlation function $\Phi(\vec{k};\ \tau)$ was obtained by calculating the temporal correlation function of the k-space domain image series, which is first calculated using a 2-D spatial Fourier transform of each image in the original microscopy time series

$$\Phi\left(\vec{k};\ \tau\right) = \tilde{i}\left(\vec{k}, t\right)\tilde{i}^{*}\left(\vec{k}, t+\tau\right), \quad (3)$$

where $\tilde{i}(\vec{k}, t)$ is the Fourier transform of the image acquired at time t, $\tilde{i}^{*}(\vec{k}, t+\tau)$ is the complex conjugate of the Fourier transform of the image acquired at time $t+\tau$, and the angular brackets denote temporal correlation.

For particles undergoing 2-D diffusion with a diffusion coefficient D, $\Phi(\vec{k};\ \tau)$ is written analytically as follows:

$$\Phi\left(\vec{k};\ \tau,\ t\right) = N\frac{q^2 I_0^2 \omega_0^4 \pi^2}{4} \times \Theta(t)\Theta(t+\tau) \times e^{\left[-\left|\vec{k}\right|^2\left(D\tau+\frac{\omega_0^2}{4}\right)\right]}, \quad (4)$$

where N is the number of fluorescent particles in the imaged region, q is the quantum yield of the fluorophore, and I_0 is the incident intensity at the center of the beam focus. Fluorophore photophysics effects (i.e., bleaching and blinking) are accounted for by the time-dependent function $\Theta(t)$.

The correlation function in Eq. 4 can be simplified to

$$\Phi\left(\vec{k};\ \tau,\ t\right) = \mathrm{N}(t)e^{\left[-\left|\vec{k}\right|^2\left(D\tau+\frac{\omega_0^2}{4}\right)\right]}, \quad (5)$$

where $\mathrm{N}(t)$ is proportional to the average number of particles in the imaged region and to the time-dependent photophysics effects given in the correlation pre-factor amplitude of Eq. 4.

In the case of two different diffusing species (1 and 2), the correlation function is the weighted sum of two contributions as follows:

$$\Phi\left(\vec{k};\ \tau,\ t\right) = \mathrm{N}_1 e^{\left[-\left|\vec{k}\right|^2\left(D_1\tau+\frac{\omega_0^2}{4}\right)\right]} + \mathrm{N}_2 e^{\left[-\left|\vec{k}\right|^2\left(D_2\tau+\frac{\omega_0^2}{4}\right)\right]}. \quad (6)$$

Although the finite width of the correlation function at zero temporal lag can potentially mask motions at spatial scales smaller than the optical PSF, the contribution of the spatial PSF can be filtered out in kICS by normalizing the correlation function to the zero temporal lag correlation function as follows:

$$\Phi\left(\vec{k};\ \tau,\ t\right) = \phi_1 e^{-\left|\vec{k}\right|^2 D_1 \tau} + \phi_2 e^{-\left|\vec{k}\right|^2 D_2 \tau}, \quad (7)$$

where ϕ_i is the amplitude of population i in the normalized multicomponent correlation function, which is proportional to N and is photophysics- and time-dependent.

This two-component model can be applied to a single species system that exhibits confined (microscale) and unconfined (macroscale) diffusion dynamics within and between small domains distributed in two dimensions. A fit to the model with a sum of two exponentials yields effective MSDs for the confined ($D_{micro}\tau$) and unconfined ($D_{macro}\tau$) populations of molecules and their respective amplitude parameters at each time lag. More specifically, the correlation function is fit with a sum of two exponentials as a function of k^2 at each temporal lag τ with fit parameters $D_{macro}\tau$, $D_{micro}\tau$, ϕ_{macro}, and ϕ_{micro} as functions of τ. MSD plots for the two populations are then constructed as $D_i\tau$-versus-τ as obtained from the fits, and the amplitude graphs are constructed from the fit-extracted values for ϕ_i-versus-τ.

The slope of the macro MSD-versus-τ plot yields D_{macro}, which is an effective diffusion coefficient of CFTR that combines its behavior both within and between microdomains as has been shown via computer simulations (Pandzic, 2013). For the image sampling rate and membrane CFTR system studied here, the slope of the first three temporal lags in the micro MSD-versus-τ plot was used to calculate D_{micro}, an effective diffusion coefficient of particles that are confined within membrane domains. The fractions within the "macro" and "micro" populations were calculated from the amplitudes at long temporal lag values (τ) as $f_{macro=\phi_{macro}/(\phi_{macro}+\phi_{micro})}$ and $f_{micro=\phi_{micro}/(\phi_{macro}+\phi_{micro})}$. According to simulations (Pandzic, 2013), the recovered values for D_{macro} and D_{micro} depend on the probability that a particle will escape from a region of confinement, and thus D_{macro} is an apparent diffusion coefficient that includes exchange into and out of those domains in addition to lateral mobility outside of the domains. On the other hand, D_{micro} is dependent on the microdomain viscosity, local interactions inside the confinement domains, and the escape probability, and therefore is independent of D_{macro}.

The y axis intercept of the micro MSD plot extrapolated from long temporal lags τ is $R^2/4$. R is a spatial "confinement" parameter that is proportional to the domain radius (d), D_{micro}, and the probability that a molecule will exit a domain (P_{out}). Based on simulations, the R value is d for domains having radii larger than the optical PSF radius (Pandzic, 2013). For those domains with radii smaller than the PSF radius, the R value is twice the pixel diameter. Recovery of the actual domain radius is limited by the background noise of the system and by spatial aliasing, which is set by the Nyquist criterion. However, simulations show that the R value and domain confinement are inversely related; i.e., the smaller the R value, the stronger the domain confinement and vice versa (Pandzic, 2013). Thus, the R value is a measure of confinement strength and not an absolute measurement of microdomain radius.

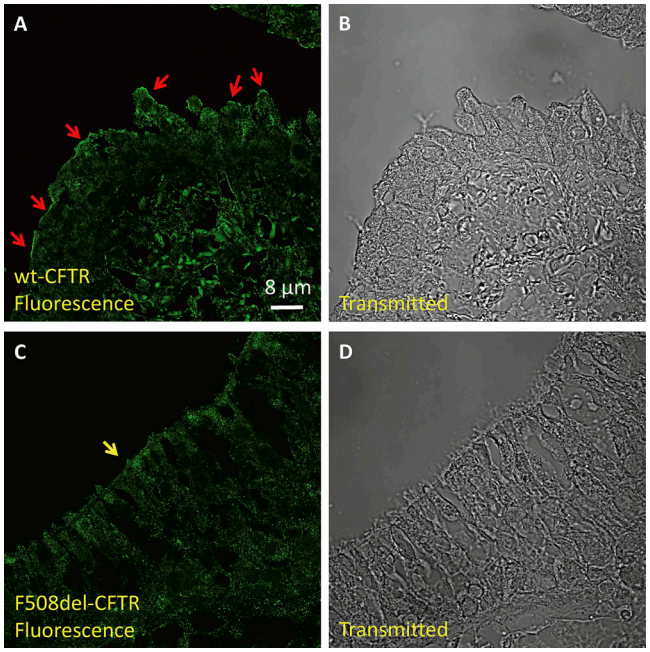

Figure S1. **CFTR distribution in bronchial tissue. (A and B)** Sections of superior bronchus were immunostained to show CFTR distribution in non-CF bronchial tissue. **(A)** Red arrows indicate apical expression of fluorescently immunostained wt-CFTR. **(B)** Transmitted light image of the same section. **(C and D)** A typical distribution of F508del-CFTR in CF bronchial tissue. **(C)** Yellow arrow points to the apical aspect. **(D)** The transmitted light image of the same section.

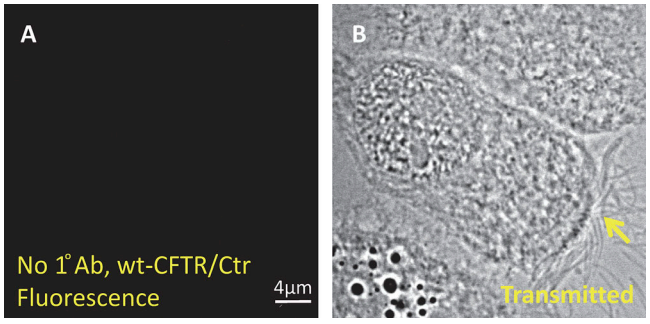

Figure S2. **F508del-CFTR distribution in differentiated and isolated pHBE cells.** pHBE cells cultured for >3 wk at the air–liquid interface, then scraped to isolate single cells and small clumps and immunostained for F508del-CFTR and centrin2. **(A)** Fluorescence confocal image of isolated pHBE cell derived from non-CF lung shows that autofluorescence is negligible when wt-CFTR is immunostained without primary anti-CFTR. **(B)** Transmitted light image of the same cell. Yellow arrow points to apical cilia.

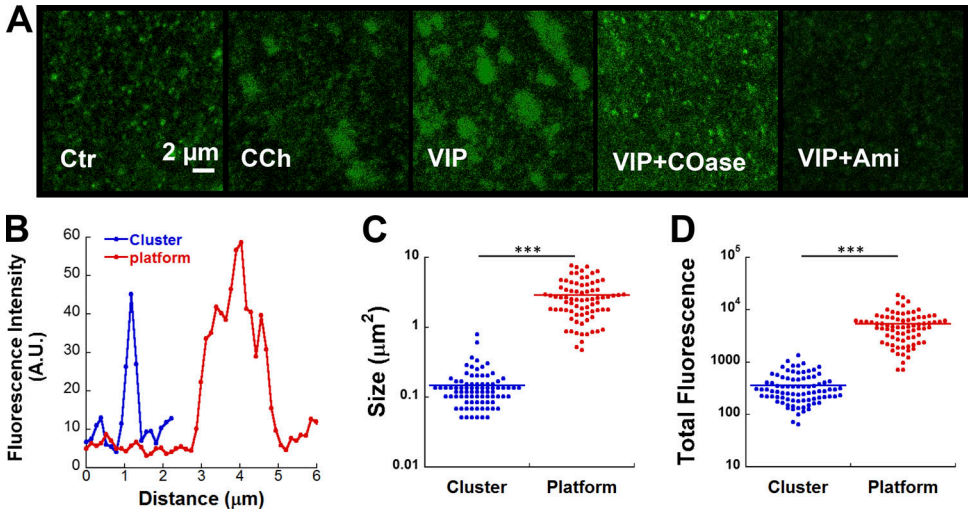

Figure S3. **Dimensions of CFTR clusters and platforms**. **(A)** pHBE cells transduced with GFP-CFTR adenovirus were imaged after 4 d under Ctr conditions and during exposure to CCh or VIP alone, to VIP after 1 h pretreatment with COase to disrupt rafts (VIP+COase), or to VIP after 40 min pretreatment with Ami to inhibit ceramide synthesis by ASMase (VIP+Ami). **(B)** Fluorescence intensity scans through a cluster (blue profile) and a platform (red profile) during VIP stimulation. **(C)** Microdomain areas in micrometers squared calculated for ∼90 individual clusters and platforms, five cells/condition. **(D)** Total fluorescence of the same areas in C showing the real aggregation state of platforms compared with clusters. A.U., arbitrary units.

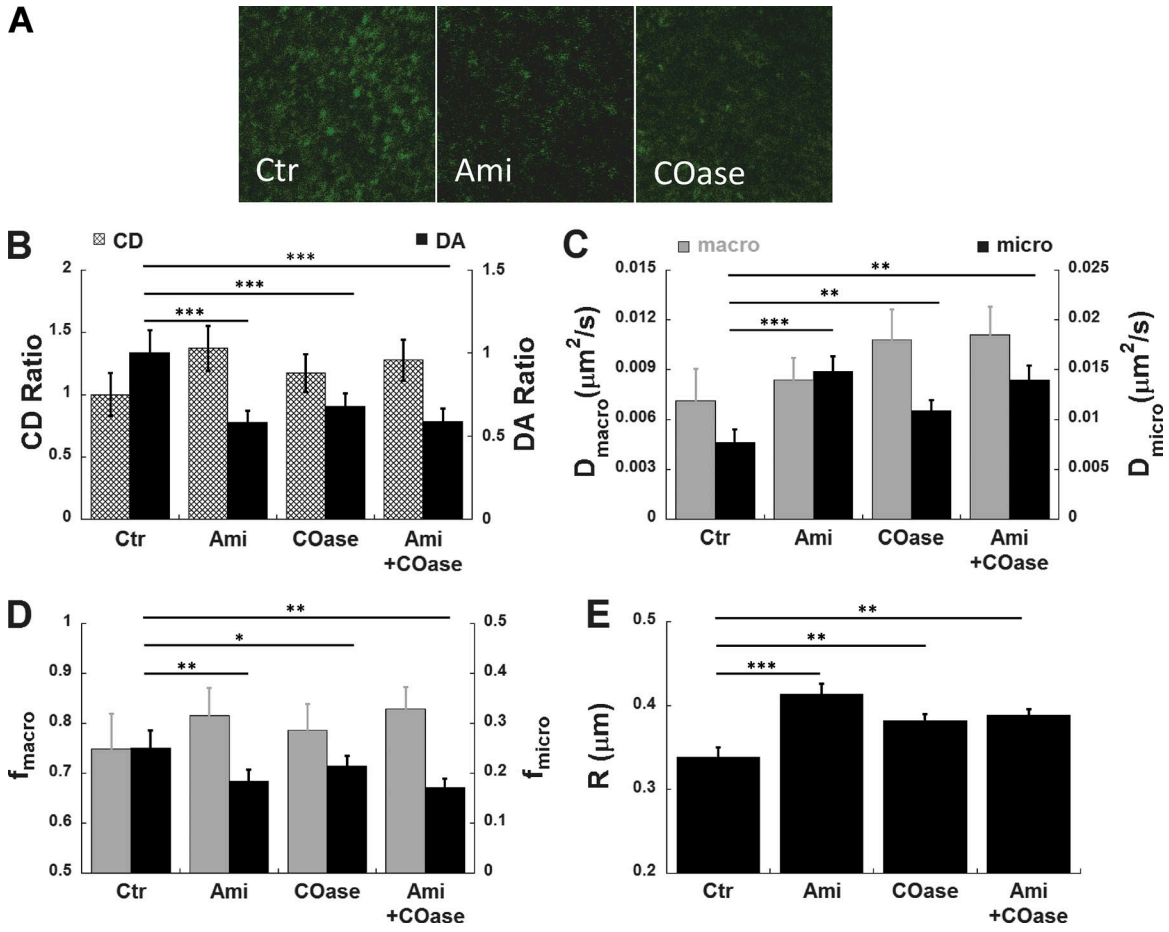

Figure S4. **CFTR dynamics are partially dependent on cholesterol and ceramide in unstimulated pHBE cells. (A)** Clusters were prevalent under Ctr conditions; however, CFTR platforms were not observed. Clustering was reduced when cells were pretreated with COase or Ami. **(B)** Quantitative analysis revealed that all three maneuvers (Ami, COase, and Ami+COase) increased CFTR CD and reduced CFTR aggregation compared with control conditions. **(C–E)** Ami and COase increased D_{macro}, D_{micro}, confined (microscopic) population fraction (f_{micro}), and confinement radius (R), indicating that cholesterol and ceramide influence CFTR dynamics under basal conditions. Mean ± SEM, ***, P < 0.001; **, P < 0.01; *, P < 0.05 (*n* = 78–80 cells each test condition, *n* = 60 control cells).

References

Abu-Arish, A., E. Pandzic, J. Goepp, E. Matthes, J.W. Hanrahan, and P.W. Wiseman. 2015. Cholesterol modulates CFTR confinement in the plasma membrane of primary epithelial cells. *Biophys. J.* 109:85–94. https://doi.org/10.1016/j.bpj.2015.04.042

Kolin, D.L., D. Ronis, and P.W. Wiseman. 2006. k-Space image correlation spectroscopy: a method for accurate transport measurements independent of fluorophore photophysics. *Biophys. J.* 91:3061–3075. https://doi.org/10.1529/biophysj.106.082768

Pandzic, E. 2013. *Measurement of protein transport and confinement in heterogeneous membranes by k-space Image Correlation Spectroscopy*. McGill, Montreal.

Wiseman, P.W., and N.O. Petersen. 1999. Image correlation spectroscopy. II. Optimization for ultrasensitive detection of preexisting platelet-derived growth factor-β receptor oligomers on intact cells. *Biophys. J.* 76:963–977. https://doi.org/10.1016/S0006-3495(99)77260-7